Solid State Communications 151 (2011) 1721–1724

Contents lists available at SciVerse ScienceDirect

Solid State Communications

journal homepage: www.elsevier.com/locate/ssc

Mass transport on adsorbate multilayers studied by surface plasmon polariton wave excitation

X. Wang, Y.Y. Fei, X.D. Zhu *

Department of Physics, University of California, Davis, CA 95616, United States

ARTICLE INFO

Article history:
Received 17 June 2011
Received in revised form
1 September 2011
Accepted 5 September 2011
by E.G. Wang
Available online 14 September 2011

Keywords:
A. Rare gas
C. Surface mass transport
C. Surface plasmon polariton wave
E. Angle resolved ellipsometry

ABSTRACT

We excited surface-plasmon polariton waves (SPPW) on Cu(111) by coupling a monochromatic optical beam with a xenon multilayer thickness grating on the metal. The SPPW excitation was detected with an angle-resolved oblique-incidence reflectivity difference technique (OI-RD). The amplitude of the resonance OI-RD signal was a quadratic function of the grating modulation depth. By monitoring the decay of the resonance OI-RD signal as a function of time and temperature, we were able to study the mass transport of xenon that plays a key role in the annealing of a "rough" Xe multilayer crystalline film.
© 2011 Elsevier Ltd. All rights reserved.

Mass transport in a film of adsorbate multilayers plays a crucial role in material synthesis, fabrication and processing. Materials grown (or synthesized) by vapor-phase deposition and those processed by ion sputtering often end with surfaces that are atomically rough [1]. To obtain an atomically flat surface with roughness less than one monolayer or one unit cell or to obtain other stable/meta-stable morphology with desirable properties, thermal annealing during and after the process is necessary, and for that the mass transport involving a host of kinetic processes need to be efficient and understood under permissible conditions. Approaches to investigating mass transport on a solid surface range from microscopic (i.e., sub-nm to nm) such as scanning probe microscopy (SPM) for real-space information [2–4] and thermal helium/electron/X-ray diffraction for k-space information [5–8], mesoscopic (tens of nm) such as LEEM and PEEM for real-space information [9], to macroscopic (sub-μm to μm) such as light scattering and diffraction for real and k-space information. Diffraction of photons or electrons or neutral atoms from a surface is routinely used to follow particular structural factors of the surface that characterize its morphology. A structural factor of a surface or a thin film is a spatial Fourier component $s(\boldsymbol{q}_s, t)$ of the height or thickness $h(x, y, t)$ with a wave vector $\boldsymbol{q}_s$ along a direction in the plane of the surface or film:

$$h(x, y, t) = \sum s(\boldsymbol{q}_s, t) \exp[i\boldsymbol{q}_s \cdot (x\hat{x} + y\hat{y})]. \quad (1)$$

The diffracted intensity $I(\boldsymbol{q}_s, t)$ of photons or electrons or neutral atoms under the condition $\boldsymbol{k}_{out} - \boldsymbol{k}_{in} = \boldsymbol{q}_s$ is proportional to $|s(\boldsymbol{q}_s, t)|^2$. $I(\boldsymbol{q}_s, t)$ is routinely measured to yield information on mass transport on solid surfaces and in thin films [5–8,10].

In this letter, we demonstrate another optical process, grating-coupled excitation of surface-plasmon polariton wave (SPPW) [11–14] on a surface that responds to $s(\boldsymbol{q}_s, t)$ of the surface in the same way as diffraction of photons or massive particles. As a result, this process can be used to study mass transport on a multilayer thin film as well. In addition to being a novel optical process for detecting $s(\boldsymbol{q}_s, t)$, the SPPW method is essentially free of the interference from diffusely scattered light from the illuminated solid surface. The scattered light has always been the challenge in the application of the linear optical diffraction technique to measurement of $s(\boldsymbol{q}_s, t)$.

Surface plasmon polariton waves (SPPW) are electromagnetic waves confined to the interface between a metal and a dielectric material. When the SPPW is excited by coupling an incident beam with a thickness-modulated thin dielectric film (grating) formed at the interface, the resonance-like dip in the angle-resolved reflectivity varies as a quadratic function of the thickness modulation depth [15]. By following the temporal evolution of the dip, one can study the mass transport on the thin film.

We excited and detected SPPW on Cu(111) with a combination of angle-resolved optical reflectivity difference technique and linear optical diffraction technique at low temperature. The grating consists of a xenon multilayer thin film epitaxially grown on Cu(111). The experimental set-up is shown in Fig. 1. A single crystal Cu(111) disk is placed inside an ultrahigh vacuum chamber

* Corresponding author. Tel.: +1 530 7524689; fax: +1 530 752 4717.
E-mail address: xdzhu@physics.ucdavis.edu (X.D. Zhu).

0038-1098/$ – see front matter © 2011 Elsevier Ltd. All rights reserved.
doi:10.1016/j.ssc.2011.09.003

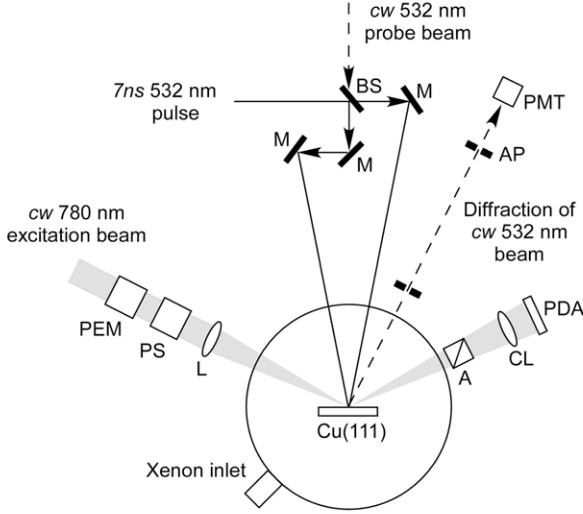

Fig. 1. Optical set-up for xenon grating-coupled excitation of SPPW on single crystalline Cu(111). M: dielectric mirrors. BS: beam splitter. PEM: photoelastic modulator. PS: phase shifter. L: spherical lens that focuses a monochromatic light beam on Cu(111) with an span of 4°. A: polarizing analyzer. CL: cylindrical lens that images the reflected light into a line across a 152-element photodiode array (PDA). AP: aperture for spatial filtering diffusely scattered light while passing the slowly focused first-order diffraction.

and cleaned with a combination of ion sputtering and thermal annealing before cooled to 38 K. We expose the metal surface to 99.999% pure xenon gas to an initial thickness d_0 determined in situ by the reflectivity difference measurement [16,17]. At 38 K adsorbed Xe atoms form a crystalline film of uniform thickness [17].

To form a grating from the uniform Xe film, we split a single 7 ns laser pulse at 532 nm to two nearly equal parts and recombine them at the Cu surface to produce an interference pattern with a periodicity of $2a = 5.45\ \mu\text{m}$ [15]. The thermal desorption produced by the interference pattern made a xenon thickness grating from the original uniform layer. At 38 K, the xenon thickness grating remains unchanged for many hours. The thickness of the grating-like Xe film can be decomposed into a Fourier series,

$$d(x) = \langle d\rangle + d_1 \cos(\boldsymbol{q}_s \cdot \boldsymbol{r}) + d_2 \cos(2\boldsymbol{q}_s \cdot \boldsymbol{r}) + \cdots \quad (2)$$

with $\boldsymbol{q}_s = (\pi/a)\hat{x}$, $s(\boldsymbol{q}_s, t) = d_1$, $s(2\boldsymbol{q}_s, t) = d_2$, and so forth. We excite the surface-plasmon polariton wave on Cu(111) using the angle-resolved oblique-incidence reflectivity difference (OI-RD) measurement with a cw diode laser at optical wavelength of $\lambda = 780$ nm. The laser beam is focused to a small spot at the center of the interference pattern with angular spread of 4°. The reflected beam is imaged onto a 152-element linear photodiode array with a cylindrical lens for angle-resolved reflectivity difference detection. The OI-RD signal, defined as $\Delta_p - \Delta_s \equiv (r_p - r_{p0})/r_{p0} - (r_s - r_{s0})/r_{s0}$ (with r_{p0} and r_{s0} being the complex reflectivity for p-polarized and s-polarized light from a bare Cu(111) while r_p and r_s the reflectivity from the Xe-covered Cu(111) [16,17], varies with the incidence angle ϕ_{inc} near the *SPR* angle ϕ_{SPR} as

$$\Delta_p - \Delta_s \cong -i\,\frac{4\pi\varepsilon_{\text{Cu}}\tan^2\phi_{inc}\cos\phi_{inc}}{(\varepsilon_{\text{Cu}}-1)(\varepsilon_{\text{Cu}}-\tan^2\phi_{inc})}\,\frac{(\varepsilon_{\text{Xe}}-\varepsilon_{\text{Cu}})(\varepsilon_{\text{Xe}}-1)}{\varepsilon_{\text{Xe}}} \times\left[\frac{\langle d\rangle}{\lambda} + \frac{g}{(\phi_{inc}-\phi_{SPR}) + i\Gamma_{SPR}}\left(\frac{d_1}{\lambda}\right)^2\right]. \quad (3)$$

$\varepsilon_{\text{Cu}} = \varepsilon'_{\text{Cu}} + i\varepsilon''_{\text{Cu}}$ and ε_{Xe} are the optical constants of Cu and bulk-phase Xe, respectively. ϕ_{SPR}, given by $\sin\phi_{SPR} = \sqrt{\varepsilon'_{\text{Cu}}/(\varepsilon'_{\text{Cu}}+1)} - \lambda/2a$, is the angle at which the SPPW is maximally excited. $\Gamma_{SPR} = \varepsilon''_{\text{Cu}}(\varepsilon'_{\text{Cu}}/(\varepsilon'_{\text{Cu}}+1) - \varepsilon'_{\text{Cu}})/2\cos\phi_{SPR}\varepsilon'^3_{\text{Cu}}\sqrt{\varepsilon'_{\text{Cu}}/(\varepsilon'_{\text{Cu}}+1)} \approx \varepsilon''_{\text{Cu}}/(2\cos\phi_{SPR}\varepsilon'^2_{\text{Cu}})$ is the half-width at half maximum (HWHM). g is a real number presently and varies weakly with ϕ_{inc} near ϕ_{SPR} [15]. Thus the real part of $\Delta_p - \Delta_s$ exhibits a resonance-like dip at $\phi_{SPR} \sim 63.7°$ at 780 nm with the maximum magnitude

$$\{\Delta_p - \Delta_s\}_{SPR,\,max} \cong -\frac{4\pi\varepsilon'_{\text{Cu}}\tan^2\phi_{inc}\cos\phi_{inc}}{(\varepsilon'_{\text{Cu}}-1)(\varepsilon'_{\text{Cu}}-\tan^2\theta_{inc})} \times \frac{(\varepsilon_{\text{Xe}}-\varepsilon'_{\text{Cu}})(\varepsilon_{\text{Xe}}-1)}{\varepsilon_{\text{Xe}}}\,\frac{g}{\Gamma_{SPR}}\left(\frac{d_1}{\lambda}\right)^2. \quad (4)$$

The quadratic dependence of OI-RD signal on the modulation depth d_1 or the structure factor $s(\boldsymbol{q}_s, t)$ is understandable from a wave-coupling argument and can be derived explicitly. Away from the resonance angle, the imaginary part of the OI-RD signal measures the mean thickness $\langle d\rangle$ in the same area,

$$\{\Delta_p - \Delta_s\}_{off\ resonance} \cong -i\,\frac{4\pi\varepsilon'_{\text{Cu}}\tan^2\phi_{inc}\cos\phi_{inc}}{(\varepsilon'_{\text{Cu}}-1)(\varepsilon'_{\text{Cu}}-\tan^2\theta_{inc})} \times \frac{(\varepsilon_{\text{Xe}}-\varepsilon'_{\text{Cu}})(\varepsilon_{\text{Xe}}-1)}{\varepsilon_{\text{Xe}}}\,\frac{\langle d\rangle}{\lambda}. \quad (5)$$

For linear optical diffraction measurement, we pass a cw probe laser beam at 532 nm along the path of one of the two 7 ns optical pulses (see Fig. 1) and monitor the diffraction from the grating with a photomultiplier after a pair of aperture. With a long focal length lens, we focus the probe beam such that after reflection the diffracted beam forms the smallest waist at the second aperture (**AP** in Fig. 1), thus minimizing the diffusely scattered light into the photomultiplier. In doing so, the probe beam covers an area slightly larger than that of the interference pattern and the diffraction signal is spatially averaged over the area. The magnitude of the n-th order diffraction from the thickness-modulated Xe film as described by Eq. (2) is as follows

$$I(n\boldsymbol{q}_s, t) = \eta\,|s(n\boldsymbol{q}_s, t)|^2 = \eta\, d_n^2. \quad (6)$$

η is a constant. In our present experiment we found that the first-order diffraction intensity $I(\boldsymbol{q}_s, t)$ was much larger than that of the second-order diffraction $I(2\boldsymbol{q}_s, t)$ so that only the first two terms in Eq. (2) were truly significant after the thickness grating was formed. Taking advantage of this fact, we deduced the modulation depth d_1 from the thickness of the initial film d_0 and the mean thickness $\langle d\rangle$ of the Xe thickness grating,

$$d_1 = d_0 - \langle d\rangle. \quad (7)$$

In Fig. 2, we show the log–log plot of $\{\Delta_p - \Delta_s\}_{SPR,\text{max}}$ measured at the resonance angle $\phi_{SPR} \sim 63.7°$ vs. the modulation depth d_1 (nm) measured at the angle away from the resonance angle. The solid line is a fit to a power law function $y(x) \sim x^\gamma$. We found the exponent γ equal to 1.95, indeed very close to 2 (see Eq. (4)).

Subsequently, we followed the evolution of $\{\Delta_p - \Delta_s\}_{SPR,\text{max}} \sim d_1^2 \sim (s(\boldsymbol{q}_s, t))^2$ at elevated temperatures to study the mass transport on the Xe multilayer film. We first formed the Xe multilayer grating on Cu(111) at 38 K, then raised the substrate temperature to a value between 47 and 53 K in a few seconds and measured the optical signal as a function of time. During the temperature change from 38 K to the set temperature and the subsequent measurement, the substrate orientation in the incidence plane was actively controlled so that the diffracted beam was maintained at the center of Aperture **AP** [18]. For diffusion measurement, the initial thickness of Xe multilayer was chosen to $d_0 = 2.13$ nm (6 monolayers). After the laser-induced desorption that formed the Xe multilayer grating, the mean thickness was typically $\langle d\rangle = 1.42$ nm (4 monolayers) so that the bare Cu surface was not exposed and the initial value of d_1 was 0.71 nm (2 monolayers). As long as the Cu surface

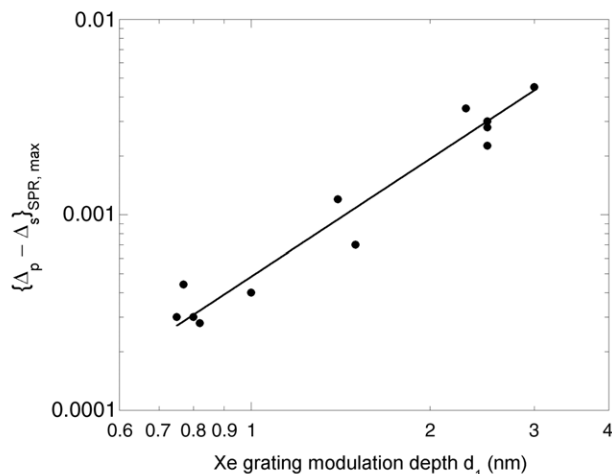

Fig. 2. Log–log plot of $\{\Delta_p - \Delta_s\}_{SPR,\max}$ measured at $\phi_{inc} = \phi_{SPR}$ vs. the modulation depth (nm) of the Xe grating. The solid line is a fit to a power law function $y(x) \sim x^{\gamma}$ with the exponent $\gamma = 1.95$, confirming the quadratic dependence of $\{\Delta_p - \Delta_s\}_{SPR,\max}$ on d_1 as described by Eq. (4).

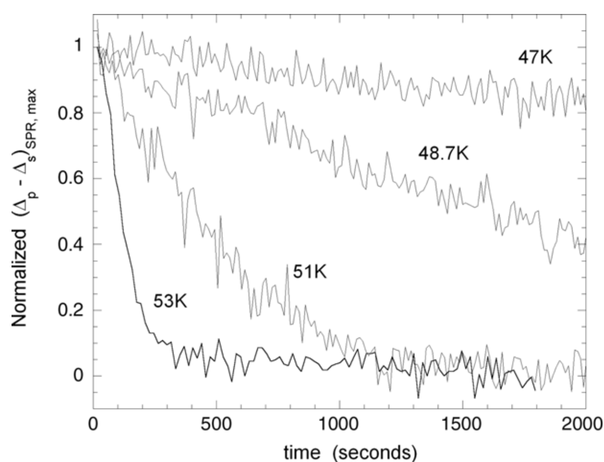

Fig. 3. Real-time decay curves of $\{\Delta_p - \Delta_s\}_{SPR,\ max} \sim d_1^2 \sim (s(\boldsymbol{q}_s, t))^2$ measured at different substrate temperatures. The temperature dependence of $s(\boldsymbol{q}_s, t)$ was subsequently fit to exponential functions $s(\boldsymbol{q}_s, t) = s(\boldsymbol{q}_s, 0)\exp(-\alpha(T)\,t)$ to obtain the decay rate constant $\alpha(T)$.

is not exposed, the results do not change with the values of d_0 and d_1 as expected.

In Fig. 3, we show a set of real-time curves of $\{\Delta_p - \Delta_s\}_{SPR,\max}$ measured at four substrate temperatures. These real-time curves display the evolution behavior of the structural factor $s(\boldsymbol{q}_s, t)$. To capture the key feature of the temperature dependence of $s(\boldsymbol{q}_s, t)$, we fit the curves to exponential functions by simply assuming $s(\boldsymbol{q}_s, t) \sim s(\boldsymbol{q}_s, 0)\exp(-\alpha(T)\ t)$. We plot the rate constant $\alpha(T)$ vs. 1000/T in Fig. 4. $\alpha(T)$ is reasonably well approximated to an Arrhenius function $\alpha(T) = \alpha_0 \exp(-E_a/k_BT)$ (solid line) characterized by an activation energy $E_a = 3.7$ kcal/mol (160 meV) and a pre-exponential factor $\alpha_0 = 7.7 \times 10^{12}$ Hz.

It would seem sensible to attribute the decay of $s(\boldsymbol{q}_s, t)$ as dominated by the diffusion of Xe monomers across the surface of the Xe multilayer film. If so we should expect $\alpha_0 = (2\pi^2/a^2)D_0$ and then arrived at $D_0 = 2.9 \times 10^4$ cm^2/s. However the activation energy and the diffusivity are both too high for intralayer and interlayer transport of Xe monomers. The activation energy for a Xe monomer hopping on open Xe(111) terraces is in the range of 10 meV, and the energy barrier for crossing a step edge (interlayer transport) is in the neighborhood of 30 meV. It means that the decay of $s(\boldsymbol{q}_s, t)$ as displayed in Fig. 3 is dominated by other kinetic

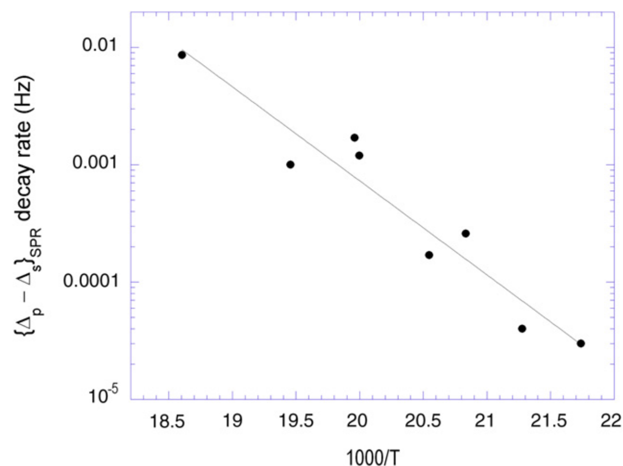

Fig. 4. Arrhenius plot of decay rate constant $\alpha(T)$ that characterize the temperature dependence $s(\boldsymbol{q}_s, t)$. The solid line is a fit to an Arrhenius function $\alpha(T) = \alpha_0 \exp(-E_a/k_BT)$ with $E_a = 3.7$ kcal/mol and $\alpha_0 = 7.7 \times 10^{12}$ Hz.

processes [19]. In fact 160 meV is close to as the experimental cohesive energy (170 meV) of bulk-phase Xe [20].

It is instructive to recognize that in addition to hopping of Xe monomers on (111) terraces of the Xe film and step-edge crossing from an upper terrace to the neighboring lower terrace, detachment of Xe from kinks and step edges of an upper terrace onto the lower terrace is another key ingredient of surface mass transport. In this case, detachment from straight step edges or kinks breaks 6–7 nearest-neighbor and 3 next-nearest neighbor "Xe–Xe" bonds that amount to 140–150 meV, in good agreement with the experimental observation. We thus arrive at a useful scenario of mass transport on a Xe multilayer film. *The thickness-modulated (non-equilibrium) form of a Xe multilayer film with an average thickness* $\langle d \rangle$ *evolves toward a uniform film through a sequence of kinetic events:* (1) *detachment of Xe monomers from kinks and long straight step edges;* (2) *hopping of monomers across open* (111) *terraces;* (3) *downward step-edge crossing from the upper terrace to the lower terrace (either directly or through atom exchange);* (4) *accommodation of Xe monomers at the step edge on top of the lowest terrace. From* 47 *to* 53 K, *the first step dominates the overall rate of mass transport*. It is noteworthy that the detachment from step edges and kinks also dominates the overall rate of thermal desorption from a Xe multilayer with thickness over 2 monolayers. Gray and coworkers found that the Xe desorption from a Xe multilayer film was of zeroth order and characterized by an apparent activation energy of 170 meV (same as the cohesive energy for bulk-phase Xe) and a pre-exponential factor of 6.5×10^{13} Hz [21].

Acknowledgment

Acknowledgment is due to the Donors of the American Chemical Society Petroleum Research Fund for the support of this research.

References

[1] J. Tersoff, A.W. Denier van der Gon, R.M. Tromp, Phys. Rev. Lett. 72 (1994) 266.
[2] Y.M. Mo, J. Kleiner, M.B. Webb, M.G. Lagally, Phys. Rev. Lett. 66 (1991) 1998.
[3] S. Horch, H.T. Lorenson, S. Helveg, E. Lægasgaard, I. Stensgaard, K.W. Jacobsen, J.K. Nørskov, F. Besenbacher, Nature 415 (2002) 891.
[4] K. Bromann, H. Brune, H. Röder, K. Kern, Phys. Rev. Lett. 75 (1995) 677.
[5] J.H. Neave, B.A. Joyce, P.J. Dobson, N. Norton, Appl. Phys. A 31 (1983) 1; P.J. Dobson, N.G. Norton, J.H. Neave, B.A. Joyce, Vacuum 33 (1983) 593.
[6] T. Sakamoto, N.J. Kawai, T. Nakagawa, K. Ohta, T. Kojima, G. Hashiguchi, Surf. Sci. 174 (1986) 651.

[7] B. Poelsema, G. Comsa, Scattering of Thermal Energy Atoms, Springer-Verlag, Berlin, 1989.
[8] E. Vlieg, A.W. Denier van der Gon, J.F. van der Veen, J.E. Macdonald, C. Norris, Phys. Rev. Lett. 61 (1988) 2241;
G. Eres, J.Z. Tischler, M. Yoon, B.C. Larson, C.M. Rouleau, D.H. Lowndes, P. Zschack, Appl. Phys. Lett. 80 (2002) 3379.
[9] J.B. Hannon, Ruud M. Tromp, Ann. Rev. Mater. Res. 33 (2003) 263.
[10] X.D. Zhu, Mod. Phys. Lett. B 6 (1992) 1217.
[11] A. Otto, Z. Phys. 216 (1968) 398.
[12] E. Kretschmann, Z. Phys. 241 (1971) 313.
[13] I. Pockrand, Surf. Sci. 72 (1978) 577.
[14] V.M. Agranovich, D.L. Mills (Eds.), Surface Polaritons: Electromagnetic Waves at Surfaces and Interfaces, North-Holland, Amsterdam, 1982.
[15] Y.Y. Fei, X. Wang, X.D. Zhu, Opt. Lett. 33 (2008) 1914.
[16] P. Thomas, E. Nabighian, M.C. Bartelt, C.Y. Fong, X.D. Zhu, Appl. Phys. A 79 (2004) 131.
[17] Y.Y. Fei, P. Thomas, X.D. Zhu, Appl. Phys. A 86 (2007) 115.
[18] X. Wang, Y.Y. Fei, X.D. Zhu, Chem. Phys. Lett. 481 (2009) 58.
[19] M. Zinke-Allmang, L.C. Feldman, M.H. Grabow, Surf. Sci. Rep. 16 (1992) 377.
[20] C. Kittel, Introduction to Solid State Physics, 7th ed., John Wiley & Sons, New York, 1996, p. 60.
[21] J. Gray, Ph.D. Thesis, University of California at Davis, 2003.